HHS Public Access

Author manuscript

Neuron. Author manuscript; available in PMC 2015 September 15.

Published in final edited form as:

Neuron. 2013 May 8; 78(3): 483–497. doi:10.1016/j.neuron.2013.02.032.

Competition Between α-Actinin and Ca^{2+}-Calmodulin Controls Surface Retention of the L-type Ca^{2+} Channel $Ca_V1.2$

Duane D. Hall[1], **Shuiping Dai**[1,±], **Pang-Yen Tseng**[2,±], **Zulfiqar Malik**[1,2], **Minh Nguyen**[2], **Lucas M. Matt**[2], **Katrin Schnizler**[1], **Andrew Shephard**[1], **Durga P. Mohapatra**[1], **Fuminori Tsuruta**[3], **Ricardo E. Dolmetsch**[3], **Carl J. Christel**[4], **Amy Lee**[4], **Alain Burette**[5], **Richard J. Weinberg**[5], and **Johannes W. Hell**[1,2,*]

[1]Department of Pharmacology, University of Iowa, Iowa City, IA 52242, USA

[2]Department of Pharmacology, University of California, Davis, CA 95615

[3]Department of Neurobiology, Stanford University, Stanford, CA 94305, USA

[4]Department of Molecular Physiology and Biophysics, University of Iowa, Iowa City, IA 52242, USA

[5]Department of Cell Biology and Physiology, University of North Carolina, Chapel Hill, NC 27599, USA

SUMMARY

Regulation of neuronal excitability and cardiac excitation-contraction coupling requires proper localization of L-type Ca^{2+} channels. We show that the actin-binding protein α-actinin binds to the C-terminal surface targeting motif of $\alpha_1$1.2, the central pore-forming Ca_V1.2 subunit, to foster its surface expression. Disruption of α-actinin function by dominant negative or shRNA constructs reduces Ca_V1.2 surface localization in HEK293 and neuronal cultures, and dendritic spine localization in neurons. We demonstrate that calmodulin displaces α-actinin from their shared binding site on $\alpha_1$1.2 upon Ca^{2+} influx through L-type channels but not through NMDAR, thereby triggering loss of Ca_V1.2 from spines. Coexpression of a Ca^{2+}-binding deficient calmodulin mutant does not affect basal Ca_V1.2 surface expression, but inhibits its internalization upon Ca^{2+} influx. We conclude that α-actinin stabilizes Ca_V1.2 at the plasma membrane, and that its displacement by Ca^{2+}-calmodulin induces Ca^{2+}-induced endocytosis of Ca_V1.2, thus providing an important negative feedback mechanism for Ca^{2+} influx.

INTRODUCTION

Voltage-dependent Ca^{2+} channels constitute a major source of Ca^{2+} influx into cells. They consist of a pore-forming α_1 subunit and auxiliary $\alpha_2\delta$, β, and γ subunits. Four genes encode

*Correspondence to jwhell@ucdavis.edu, (530) 752-6540.
±Co-first authors

α_1 subunits ($\alpha_1$1.1–1.4) that give rise to the dihydropyridine-sensitive L-type Ca^{2+} channels Ca_V1.1–1.4. The auxiliary subunits facilitate release from the endoplasmic reticulum (ER) by inhibiting ubiquitination and proteasomal degradation and influence electrophysiological properties of Ca^{2+} channels such as activation and inactivation (Altier et al., 2011; Dai et al., 2009; Dolphin, 2009; Waithe et al., 2011). Ca_V1.2 is the main L-type channel in brain (Hell et al., 1993b; Sinnegger-Brauns et al., 2004) and heart (Seisenberger et al., 2000). Ca_V1.2 is important for numerous neuronal functions, including synaptic plasticity (Moosmang et al., 2005) (Qian and Hell, unpublished), learning and memory (Moosmang et al., 2005), and gene expression (Dolmetsch et al., 2001; Graef et al., 1999). Ca_V1.2 is enriched at postsynaptic sites (Davare et al., 2001; Hell et al., 1996; Obermair et al., 2004; Tippens et al., 2008) (see also (Higley and Sabatini, 2008; Hoogland and Saggau, 2004)). Precise subcellular localization of Ca_V1.2 is important for generating Ca^{2+} nanodomains that control excitability (Berkefeld et al., 2006; Liu et al., 2004; Marrion and Tavalin, 1998) and long-term potentiation (Grover and Teyler, 1990). Auxiliary subunits promote surface expression of Ca_V1.2, but the molecular mechanisms that determine the precise subcellular localization of Ca_V1.2 are unknown.

Dihydropyridine binding to L-type channels in the plasma membrane of intact GH4C1 cells decreases upon K^+-induced depolarization in a dose- and time-dependent manner but reappears within minutes upon return to basal [K^+] (Liu et al., 1994). Similar activity-dependent internalization of Ca_V1.2 occurs in cultured cortical neurons (Green et al., 2007). Disruption of F-actin decreases L-type currents in neurons (Johnson and Byerly, 1993), cardiomyocytes (Dzhura et al., 2002; Lader et al., 1999), and vascular smooth muscle cells (Nakamura et al., 2000). The activity of other ion channels, such as the NMDAR, also decreases upon actin depolymerization (Rosenmund and Westbrook, 1993). The actin-binding protein α-actinin, which links filamentous actin to integral membrane proteins, binds directly to NMDAR and disruption of this interaction reduces NMDAR channel activity (Krupp et al., 1999; Wyszynski et al., 1997; Zhang et al., 1998). We now report that α-actinin binds to residues 1584 to ~1670 in the proximal C-terminus of rabbit $\alpha_1$1.2. Earlier independent work found that deletion of residues 1623–1666 impairs surface expression of Ca_V1.2 (Gao et al., 2000) (see also (Kepplinger et al., 2000)). This region includes the IQ segment (residues 1644–1666), which mediates Ca^{2+}-dependent inactivation (CDI) by binding to Ca^{2+}-CaM (Fallon et al., 2005; Kim et al., 2004; Peterson et al., 1999; Van Petegem et al., 2005; Zhou et al., 1997; Zuhlke et al., 1999). Recent evidence suggests that overexpression of CaM can support trafficking of Ca_V1.2 to the cell surface in heterologous expression systems, perhaps by helping to mask an ER retention signal within the quaternary structure of Ca_V1.2 for forward trafficking (Ravindran et al., 2008; Wang et al., 2007). However, it is unclear whether endogenous CaM promotes Ca_V1.2 surface expression in neurons. Most importantly, it is unknown how Ca_V1.2 is retained at the cell surface and targeted to specific locations in the plasma membrane where Ca_V1.2 accumulation is required, such as postsynaptic sites.

We show that α-actinin binds to the membrane targeting and CaM-binding region in the $\alpha_1$1.2 C-terminus and fosters Ca_V1.2 surface expression in HEK293 cells and neurons. CaM competes with α-actinin for $\alpha_1$1.2 binding in the presence but not absence of Ca^{2+}. Ca^{2+} influx triggers displacement of α-actinin from Ca_V1.2 by Ca^{2+}/CaM, which results in loss of

$Ca_V1.2$ from the cell surface and dendritic spines if lasting long enough for endocytosis to occur.

RESULTS

$Ca_V1.2$ Interacts with α-Actinin in Brain

Previous work (Lu et al., 2007) suggests that α-actinin and $Ca_V1.2$ interact, which was evaluated by co-immunoprecipitation (coIP) and immunofluorescence microscopy (IF). The antibodies CNC1 and FP1 against $\alpha_1$1.2 specifically recognize the full length form of $\alpha_1$1.2 (~240 kDa apparent M_R) and a C-terminally truncated form (~200 kDa) generated by proteolytic processing (Davare et al., 2001; Hell et al., 1996; Hell et al., 1993a; Hell et al., 1993b). Their specificity for immunofluorescence staining was confirmed by comparing untransfected HEK293 cells with those transfected with either $\alpha_1$1.2 or $\alpha_1$1.3 (Figure S1A). Because these antibodies are highly selective for $\alpha_1$1.2 and directed against the same region of $\alpha_1$1.2, they were used interchangeably throughout the study. The isoform selectivity of the two widely used monoclonal antibodies BM-75.2 and EA-53 against α-actinin was similarly defined (Figure S1B,C). Four different genes encode four highly homologous α-actinin isoforms. BM-75.2 recognizes α-actinin-1 through -4 equally well by immunoblotting (IB) but α-actinin-1 selectively by immunofluorescence (IF). EA-53 interacts preferentially with α-actinin-2 by IB but with α-actinin-2 through -4, though not -1, by IF. BM-75.2 was thus primarily used, and supplemented with EA-53 for IF experiments to detect all isoforms.

CoIP of α-actinin and $Ca_V1.2$ was observed from solubilized rat forebrain (Figure 1A bottom, lane 3; Figure 8A, lanes 1–6). This CoIP was specific as it was absent in control IgG antibody samples (Figure 1A, lane 2; Fig. 8A, lanes 7 and 8). The two main size forms of $\alpha_1$1.2 often appear as multiple partially resolved bands due to splice variations (Figure 1A top). IF labeling of rat brain sections showed extensive colocalization of $Ca_V1.2$ puncta and α-actinin puncta in cortical neurons (Figure 1B). Both $\alpha_1$1.2 and α-actinin were detected within somata of pyramidal neurons and their dendritic arbors. Colocalization between $\alpha_1$1.2 and α-actinin was also observed in the dendrites of neurons in primary hippocampal cultures (see Figure S4). High magnification clearly illustrates overlapping punctate staining for $\alpha_1$1.2 and α-actinin (Figure 1C). Many of these puncta are likely synapses, as both $Ca_V1.2$ (Davare et al., 2001; Hell et al., 1996; Obermair et al., 2004; Tippens et al., 2008) and α-actinin (Allison et al., 1998; Wyszynski et al., 1998; Wyszynski et al., 1997) are mostly clustered at postsynaptic sites.

α-Actinin Binds to the CaM Binding and Surface Targeting Region of $\alpha_1$1.2

To confirm the $\alpha_1$1.2 - $Ca_V1.2$ interaction and to obtain potential leads for its physiological functions we determined the α-actinin binding site on $\alpha_1$1.2 by pull down experiments. Intracellular N- and C-termini and loops between the 4 homologous membrane domains (Figure 2A) were expressed in *E. coli* as GST-fusion proteins and immobilized on glutathione-Sepharose. The C-terminus of $\alpha_1$1.2 was divided into several overlapping fragments (Figure 2B). The overlapping $\alpha_1$1.2 C-terminal fragments CT-A and CT-1, but no other fusion protein, pulled down α-actinin from brain homogenates (Figure 2C, top).

Probing of the lower portion of the blots with anti-GST antibody indicates that comparable amounts of the various fusion proteins were present in the different pull down samples (Figure 2C, bottom). The cDNA in our GST-CT-A plasmid covers residues 1584–1707 with GST being placed at the N-terminus of this fragment. C-terminal truncation of 40 residues of GST-CT-A as suggested by GST probing (Figure 2C, bottom) would retain residues 1584–1667 including residues 1623–1666, which are critical for proper trafficking of $Ca_V1.2$ to the cell surface (Gao et al., 2000). Some of the $\alpha_1$1.2-derived GST-fusion proteins were also incubated with purified maltose binding protein (MBP) - α-actinin-1 expressed in *E. coli* (Figure 2D). Again, CT-A, but none of the other GST fusion proteins, recruited α-actinin indicating a direct interaction. Further extensive binding studies showed that α-actinin can bind independently with 3 different sites to residues 1588–1609, 1614–1635, and 1644–1670, with the latter being of very high affinity (apparent Kd: 3.5±0.5 nM) and sensitive to displacement by Ca^{2+}/CaM (Malik, Shea, and Hell, unpublished data).

Functional Interaction of α-Actinin and $Ca_V1.2$ in HEK293 Cells

$\alpha_1 1.2_{1623–1666}$ also binds CaM, which mediates CDI of $Ca_V1.2$. Similarly, CaM and α-actinin bind to overlapping sites on the NMDAR and mediate its Ca^{2+}-dependent desensitization (Krupp et al., 1999; Leonard et al., 2002; Merrill et al., 2007; Wyszynski et al., 1997; Zhang et al., 1998). We therefore tested whether α-actinin controls $Ca_V1.2$ functions. The α-actinin head consists of two calponin homology (CH) domains followed by a rod domain that consists of four spectrin repeats (SR) (Fig. 2E). The head as well as the rod domain can act in a dominant negative fashion (Pavalko and Burridge, 1991; Schnizler et al., 2009; Zhang and Gunst, 2006). Furthermore, the CH and SR domains can independently interact with $\alpha_1 1.2_{1623–1666}$ (Malik, Shea, and Hell, unpublished data). Accordingly, the Head and Rod domain have the potential to exert a dominant negative effect by disrupting the interaction between $\alpha_1 1.2_{1623–1666}$ and endogenous α-actinin.

Contrary to our initial hypothesis, coexpression of the Head or Rod domain of α-actinin-1, which was tagged with EGFP, did not alter activation or inactivation of either Ba^{2+} or Ca^{2+} currents through $Ca_V1.2$ (Figure 3A,B,E,F). Current-voltage relationships and steady-state inactivation were also unaffected (Figure 3C,D). However, the density of Ba^{2+} current through $Ca_v1.2$ was significantly reduced by both constructs (Figure 3C). Because such a reduction in current density could be due to a decrease in surface localization of $Ca_v1.2$, we quantified this parameter by surface biotinylation. HEK293 cells were cotransfected with $Ca_V1.2$ containing an HA-tagged variant of $\alpha_1$1.2 (Obermair et al., 2004) and EGFP-head, EGFP-rod or EGFP alone before surface biotinylated. $\alpha_1$1.2 was extracted before IP and IB with anti-$\alpha_1$1.2 to measure total $\alpha_1$1.2 levels, and re-probed with Streptavidin-HRP to measure levels of $\alpha_1$1.2 at the cell surface. Head and Rod domain significantly decreased $\alpha_1$1.2 biotinylation (Figure 3G,H) indicating a reduction in $Ca_V1.2$ surface expression.

To control for perturbation of cortical F-actin by these constructs, parallel cultures were stained with phalloidin, which specifically binds to F-actin. Cortical actin structures were intact in cells transfected with either the Head or Rod domain, though the EGFP-Head domain formed intracellular clusters that also stained for F-actin (Figure S2). As we did not observe a detectable change in cortical F-actin with the Head construct, the Head domain

clusters may sequester some F-actin in the cell interior without causing a substantial alteration in the content of dynamic and cortical actin. Modest amounts of the head domain outside the clustered structures apparently suffice to act as dominant negative constructs without grossly disturbing cortical F-actin. The EGFP-Rod domain, which does not bind F-actin, showed a diffuse distribution and did not colocalize with F-actin, as expected (Pavalko and Burridge, 1991; Zhang and Gunst, 2006). Accordingly, the effects of the Head and Rod domains on $Ca_V1.2$ surface expression are not due to disruption of F-actin.

The above electrophysiological, IF, and IP experiments indicate that the dominant negative α-actinin constructs reduce surface expression of $Ca_V1.2$ in HEK293 cells under equilibrium conditions.

Knockdown of α-Actinin Reduces $Ca_V1.2$ Surface Expression in HEK293 Cells

We performed knock down experiments to further test the role of α-actinin. We developed shRNA expressing vectors that specifically and individually knocked down the different α-actinin isoforms in humans and rodents (Table S1). To test these constructs, we expressed EGFP-tagged α-actinin-1 through -4 with or without the corresponding shRNA. Coexpression of each shRNA decreased the EGFP-α-actinin band of the respective isoform (Figure 4A) but not of other isoforms (Schnizler et al., 2009). RT-PCR showed that HEK293 cells express α-actinin-1 and -4, but not -2 or -3 (Figure S3A). Coexpression of shRNAs against these two α-actinins in HEK293 cells decreased $Ca_V1.2$ peak currents when compared to coexpression of shRNAs against α-actinins-2 and -3, which served as negative controls (Figure 4D). α-Actinin-1 plus -4 shRNA expression did not affect activation or inactivation with either Ba^{2+} or Ca^{2+} as charge carrier (Figure 4B,C,E,F,G). Parallel cultures were labeled with phalloidin to verify that α-actinin-1 and -4 knock-down had no significant effect on cortical F-actin. Cells transfected with the shRNA vectors against α-actinin-1 and -4 showed virtually the same pattern of cortical F-actin staining as their untransfected neighbors and as cells transfected with either the parental pSilencer-DsRed vector or vectors against α-actinin-2 and -3 (Figure S3B).

Knockdown of α-Actinin Impairs Synaptic Localization of $Ca_V1.2$

$Ca_V1.2$ (Bloodgood and Sabatini, 2007; Davare et al., 2001; Hell et al., 1996; Obermair et al., 2004; Tippens et al., 2008) and α-actinin (Allison et al., 1998; Wyszynski et al., 1998; Wyszynski et al., 1997) are enriched in postsynaptic dendritic spines, where they colocalize (Figure 1, S4). We found by RT-PCR that neurons express α-actinins-1, -2, and -4 (Schnizler et al., 2009) (see also (Peng et al., 2004; Walikonis et al., 2000; Walikonis et al., 2001; Wyszynski et al., 1998)). To examine the role of α-actinin in neurons, hippocampal cultures were transfected after 4 days in vitro (DIV) with parental pSilencer (pSil), a combination of shRNA expressing vectors against α-actinins-1, -2 and -4, or against α-actinin-3 as negative control. At 21 DIV colocalization of endogenous $\alpha_1 1.2$ and the postsynaptic markers PSD-95 (Tseng and Hell, unpublished data) and Shank were significantly reduced upon knock-down compared to control (empty pSil plasmid or α-actn-3 shRNA) (Figure 5). Ectopic expression of α-actinin-1 with silent shRNA-resistant mutations completely rescued the loss of $\alpha_1 1.2$ from spines.

CaM Competes with α-Actinin for the $\alpha_1$1.2 C-terminus in a Ca^{2+}-dependent Manner

Because α-actinin binds to the same region of $\alpha_1$1.2 as CaM, we tested whether the two proteins compete for binding to this site. As before (Figure 2C, lane 6), MPB-tagged α-actinin-1 bound to immobilized CT-1-GST (Figure 6A, lane 1) but not to GST alone (lanes 5–8). Addition of Ca^{2+}-free CaM ("apo-CaM") or Ca^{2+} individually did not alter α-actinin-1 binding (lanes 2,3), but Ca^{2+} and CaM together displaced α-actinin-1 from GST-CT-1 (lane 4). Endogenous α-actinin co-precipitated with $\alpha_1$1.2 from brain extracts in the absence but not presence of free Ca^{2+} (Figure 6C), as endogenous CaM likely displaced α-actinin from the $\alpha_1$1.2 complex when Ca^{2+} was available. Like Ca^{2+}-CaM, apo-CaM also binds to the IQ locus in the C-terminus of $\alpha_1$1.2, but with much lower affinity, indicating that CaM rearranges itself on the $\alpha_1$1.2 C-terminus upon addition of Ca^{2+} to form additional interactions that stabilize the association ((Halling et al., 2006) and Ref therein). Furthermore, apo-CaM and α-actinin can simultaneously bind GST-CT-1 (Malik, Shea, and Hell, unpublished data). These observations suggest that apo-CaM, $\alpha_1$1.2, and α-actinin form a ternary complex under low basal intracellular Ca^{2+} conditions. When Ca^{2+} concentrations increase, CaM binds Ca^{2+} and displaces α-actinin from $\alpha_1$1.2 (Figure 9H, upper panels).

Ca^{2+} Influx Induces Ca_V1.2 Internalization

If this Ca^{2+}-dependent displacement of α-actinin occurred in intact cells, it would sever the interaction between Ca_V1.2 and its surface anchor, α-actinin, triggering the reversible removal of L-type channels from the cell surface upon elevation of intracellular Ca^{2+} described earlier (Green et al., 2007; Liu et al., 1994). To test this hypothesis, HEK293 cells expressing Ca_V1.2 were treated with the Ca^{2+} ionophore ionomycin or the L-type channel activity-enhancing BayK8644 for 10 min before surface biotinylation. Both 10 μM ionomycin and BayK8644 clearly reduced surface biotinylation of $\alpha_1$1.2 (Figure 7A, top left panel, lanes 2 and 3) without affecting total amounts of $\alpha_1$1.2 detected in lysate samples (top right). Accordingly, $\alpha_1$1.2 had redistributed away from the cell surface without being degraded. The relative levels of isolated and total biotinylated proteins were similar, as indicated by the streptavidin reprobing (Figure 7A bottom). Intracellular proteins were not biotinylated, as indicated by the α-actinin blots (Figure 7A middle left). The small amount of α-actinin in the streptavidin pull-downs likely reflects its interaction with various surface proteins such as integrins.

To determine whether Ca^{2+} influx through Ca_V1.2 triggers endocytosis in neurons, mature rat cortical cultures (21 DIV) were treated for 10 min with either ionomycin or BayK8644 and surface proteins cross-linked with the membrane impermeant crosslinker BS^3 (Boudreau and Wolf, 2005; Grosshans et al., 2002). Equivalent amounts of protein in lysates were separated on SDS-PAGE gels and immunoblotted for $\alpha_1$1.2 (Figure 7B, top) or the transferrin receptor (TfR) as a control (Figure 7B, bottom). $\alpha_1$1.2 and TfR in lysates from cultures that had not been crosslinked were of the expected molecular mass (M_R), including long and short $\alpha_1$1.2 forms, which appear as weak bands due to low endogenous expression (Figure 7B, top). BS^3 resulted in a reduction of the free $\alpha_1$1.2 long and short forms and a concomitant increase in higher M_R species at the top of the gel (Figure 7B top, second lane). A modest amount of the TfR was also crosslinked and migrated in two clearly detectable

bands above the non-crosslinked form. Ionomycin or BayK8644 induced re-appearance of non-crosslinked $\alpha_1$1.2 long and short forms, indicating that more Ca_V1.2 had become inaccessible to BS^3 due to endocytosis upon Ca^{2+} influx. BayK8644 increases Ca^{2+} flux by L-type channels by 2–3 fold, matching physiological increases during heightened neuronal activity (Tavalin et al., 2004; Xu et al., 2010). Thus we tested more systematically whether BayK8644 reduces surface localization of Ca_V1.2, which was the case (Figure 7C, $p<0.05$).

To investigate whether Ca^{2+} influx leads to Ca_V1.2 endocytosis in hippocampal neurons by CaM-dependent displacement of α-actinin, we heterologously expressed $\alpha_1$1.2 with an extracellular HA tag and an N-terminal YFP tag (Green et al., 2007). Cells were surface labeled with anti-HA and the ratio of HA to YFP signal monitored following membrane depolarization. Depolarization for 15 min with 65 mM KCl reduced this ratio by 40–60%, indicating that it triggered endocytosis of Ca_V1.2 (Figure 7D–F). Expression of a CaM mutant that contained a point mutation in each of its 4 EF hands to abrogate Ca^{2+} binding (CaM_{1234}) prevents endogenous CaM from causing CDI of Ca_V1.2 (Peterson et al., 1999; Pitt et al., 2001) (see also Figure 9E vs F). CaM_{1234} did not affect basal Ca_V1.2 surface expression but averted internalization of Ca_V1.2 upon membrane depolarization (Figure 7D,E). This effect was not due to excess CaM per se, as overexpression of WT CaM had no effect. These results reveal a new physiological role for Ca^{2+} and CaM in dynamically regulating Ca_V1.2 surface localization after insertion into the plasma membrane.

We used the same approach to evaluate the role of α-actinin in Ca_V1.2 surface targeting under basal and depolarizing conditions by knocking down α-actinin-1, -2, and -4. Neurons were cotransfected with the combination of the corresponding shRNA vectors plus YFP- and HA-tagged $\alpha_1$1.2. Knockdown reduced basal Ca_V1.2 surface expression and KCl-induced reduction in plasma membrane Ca_V1.2 (Figure 7F). Some KCl-triggered Ca_V1.2 endocytosis appears to have remained (although it did not reach statistical significance) likely due to incomplete α-actinin knock-down. Cotransfection with shRNA against α-actinin-3, which is not present in neurons, affected neither surface expression nor depolarization-induced internalization of Ca_V1.2, compared to non-shRNA plasmid controls.

Off-target effects of shRNAs were excluded by rescue. Overexpression of WT α-actinin-1 together with YFP- and HA-tagged $\alpha_1$1.2 led to a small, statistically insignificant increase in Ca_V1.2 surface expression (Figure 7G). Knockdown of neuronal α-actinins with a combination of shRNAs against α-actinin-1, -2, and -4, which also knocks down the ectopically expressed α-actinin-1, reduced surface expression of YFP- and HA-tagged $\alpha_1$1.2 by 30–40% whether wt α-actinin-1 was or was not co-expressed. For the rescue experiment, silent mutations were introduced into the shRNA recognition site of α-actinin-1 to prevent silencing. Neurons expressing shRNA-insensitive α-actinin-1 showed a small, statistically insignificant increase in Ca_V1.2 surface expression similar to neurons transfected with the unmodified α-actinin-1 (Figure 7G). Expression of this shRNA-insensitive α-actinin-1 prevented the reduction of surface expression of Ca_V1.2 by α-actinin knock down. We conclude that the shRNA effects are specific and that the α-actinin-1 isoform is sufficient for proper surface expression of Ca_V1.2.

Ca^{2+} Influx Displaces α-Actinin from $Ca_V1.2$ in Acute Forebrain Slices

Like BayK8644, FPL64176 increases Ca^{2+} flux through L-type channels by 2–3 fold but by a different mechanism (Tavalin et al., 2004; Xu et al., 2010; Zhang et al., 2011). Incubation of acute forebrain slices with ionomycin, glutamate, or FPL reduced α-actinin coIP with $Ca_V1.2$ by >50% (Figure 8A,B). Remarkably, the glutamate effect was completely blocked by the L-type antagonist isradipine but not by two different NMDAR antagonists (pore blocking MK801 and glycine competing 5,7-dichlorokynurenic acid (DCKA); Figure 8B,C; we confirmed activity of the MK801 batch by testing its effect on LTP, which was blocked; Qian and Hell, unpublished). Accordingly, induction of massive Ca^{2+} influx via NMDAR by glutamate does not contribute to $Ca_V1.2$ endocytosis, which is rather specifically triggered by Ca^{2+} influx through L-type channels even though a substantial portion of L-type channels resides in dendritic spines where NMDAR are also concentrated (Figure 1B,C) (Davare et al., 2001). FPL prolongs L-type channel openings but does not itself open the channels and thus depends on network activity. α-Actinin - $Ca_V1.2$ CoIPs indicate that inhibition of network activity with either the Na^+ channel blocker TTX or the AMPAR antagonist NBQX prevented the dissociation of α-actinin from $Ca_V1.2$ by FPL treatment (Figure 8D). FPL treatment as short as 60 s was sufficient to displace α-actinin from $Ca_V1.2$ (Figure 8E). Accordingly, an increase of Ca^{2+} influx through L-type channels within physiological range is sufficient to displace α-actinin from $Ca_V1.2$. Furthermore, dissociation of α-actinin from $Ca_V1.2$ by FPL treatment was blocked by three different CaM antagonists (W7, trifluoperazine (TFP), calmidazolium (CMZ); Figure 8F). Although none of those drugs are entirely specific for CaM, they differ in their side effects (detailed in (Bartos et al., 2010)). Collectively these data thus indicate that removal of α-actinin from $Ca_V1.2$ requires CaM.

Ca^{2+} Influx Displaces $Ca_V1.2$ from Dendritic Spines

Like slices, hippocampal cultures were treated with FPL and glutamate to enhance basal L-type-mediated Ca^{2+} influx and network activity, respectively. Cultures were then analyzed by IF triple labeling for endogenous $Ca_V1.2$, the presynaptic marker bassoon, and the postsynaptic marker Shank to define postsynaptic $Ca_V1.2$ puncta. FPL and glutamate incubations lead to a statistically highly significant reduction in co-localization of $Ca_V1.2$ with Shank (Figure 9A,B). The AMPAR antagonist NBQX, which blocks the spontaneous synaptic and thereby neuronal activity in these cultures, inhibits FPL-induced loss of $Ca_V1.2$ from spines. Accordingly, network activity is required for the FPL effect. We conclude that Ca^{2+} influx via L-type channels induces loss of $Ca_V1.2$ from spines.

Ca^{2+} Influx Causes Run-down of L-type Currents by CaM-dependent Endocytosis of L-type Channels

Endocytosis of $Ca_V1.2$ upon Ca^{2+} influx should result in loss of L-type currents ($I_{Ca,L}$). In fact, whole cell patch recordings of $I_{Ca,L}$ upon 100 ms depolariziations at 0.2 Hz with extracellular Ca^{2+} in hippocampal cultures showed a strong run down over 5 min (Figure 9D,E). N- and P/Q-type Ca^{2+} currents were blocked by ω-Conotoxin (CTx) GVIA and MVIIC to effectively isolate $I_{Ca,L}$ as indicated by its complete elimination by isradipine (Figure 9C). The run down of $I_{Ca,L}$ was largely abrogated by CMZ and ectopic expression of

the Ca^{2+} -binding deficient CaM_{1234} mutant (Figure 9D,F), which also blocked CDI (Figure 9F) as expected (Peterson et al., 1999). The inactivation remaining in CaM_{1234}-transfected neurons reflects Ca^{2+}/CaM-independent voltage-dependent inactivation (VDI). To confirm that run down was due to endocytosis rather than induction of long lasting silent states of the L-type channels, we included dynasore, an endocytosis inhibitor, in the recording electrode. Dynasore also inhibited the run down. Importantly, none of the treatments reduced peak currents (Figure 9G) excluding the possibility that such a reduction could have resulted in decreased run-down. These data indicating that the Ca^{2+} influx through L-type channels triggers endocytosis of $Ca_V1.2$ via CaM.

DISCUSSION

Surface expression of $Ca_V1.2$ depends on the efficacy of trafficking of this channel from the ER to the plasma membrane and how well it is retained there. The auxiliary $\alpha_2\delta$ and β subunits and, when overexpressed, CaM can promote trafficking of $Ca_V1.2$ to the surface, probably by facilitating its release from the ER (Dai et al., 2009; Dolphin, 2009; Ravindran et al., 2008; Wang et al., 2007). How $Ca_V1.2$ is anchored at defined surface localizations has hitherto been unknown. Pull down assays show that α-actinin binds at or near the IQ motif in $\alpha_1$1.2 (residues 1644–1666; Figure 2). Surface and IF labeling upon expression of dominant negative fragments of α-actinin and knock down of α-actinin show that α-actinin localizes $Ca_V1.2$ in the plasma membrane and dendritic spines (Figures 3–5), possibly by linking $Ca_V1.2$ to F-actin as depolymerization of F-actin causes a run down of L-type current (Johnson and Byerly, 1993). Accordingly, mutations in the shared CaM/α-actinin binding region of $\alpha_1$1.2 that impair surface expression of $\alpha_1$1.2 (Ravindran et al., 2008; Wang et al., 2007) likely act by affecting α-actinin rather than CaM binding.

CaM pre-associates in its Ca^{2+}-free apo form with the IQ motif of $\alpha_1$1.2 to mediate rapid CDI (Fallon et al., 2005; Kim et al., 2004; Peterson et al., 1999; Van Petegem et al., 2005; Zuhlke et al., 1999). Given that the interaction between CaM and the IQ region controls channel inactivation, binding of α-actinin to this region could also affect gating. However, neither overexpression of the dominant negative α-actinin Head or Rod domain (Figure 3) nor knockdown of α-actinin altered activation or inactivation of Ca^{2+} or Ba^{2+} currents through $Ca_V1.2$ (Figure 4). It thus appears that α-actinin does not affect the structural determinants of $Ca_V1.2$ gating. However, if α-actinin is absolutely essential for $Ca_V1.2$ surface expression, the currents through $Ca_V1.2$ that remain after expression of α-actinin shRNA or dominant negative constructs would reflect $Ca_V1.2$ that maintained binding to endogenous α-actinin that escaped knock-down or that successfully competed with the dominant negative rod or head domain. Accordingly, the remaining channels would not be different from $Ca_V1.2$ under control conditions. We thus cannot exclude that α-actinin affects channel properties.

α-Actinin binds to the IQ motif simultaneously with CaM only in the absence but not presence of Ca^{2+} (Figure 6; Malik, Shea, and Hell, unpublished data). These results indicate that under basal conditions α-actinin and CaM are both associated with the IQ region of native $\alpha_1$1.2 (Figure 9H). Ca^{2+} in conjunction with CaM displaces α-actinin from the IQ motif in vitro (Figure 6) and from endogenous $Ca_V1.2$ in intact neurons (Figure 8). Ca^{2+}

influx decreases surface expression of $Ca_V1.2$ in HEK293 cells (Figure 7A) and neurons in a CaM-dependent manner (Figure 7B–E). Also, earlier work on the functional coupling between L-type channels and Ca^{2+}-activated K^+ channels found that chelating intracellular Ca^{2+} with BAPTA increases the prevalence of L-type channels at the surface of hippocampal pyramidal neurons over a period of 30 min (Marrion and Tavalin, 1998). This earlier work provides independent support for a role of intracellular Ca^{2+} in regulating abundance of L-type channels in the plasma membrane.

Ca^{2+}-induced binding of eIF3e to loop II/III in $Ca_v1.2$ is important for Ca^{2+}-driven endocytosis of $Ca_v1.2$ (Green et al., 2007). It is possible that displacement of α-actinin by Ca^{2+}/CaM from the C-terminus of $Ca_v1.2$ and eIF3e binding to loop II/III of $Ca_v1.2$ are two completely independent yet individually necessary steps for endocytosis of $Ca_v1.2$ to occur. Alternatively, the conformational change of the C-terminus of $Ca_v1.2$ that results from Ca^{2+} associating with CaM could affect the conformation of loop II/III and thereby binding of loop II/III to eIF3e, linking the two events. It is also possible that α-actinin bound to the C-terminus of $Ca_v1.2$ obstructs access of eIF3e to loop II/III until α-actinin is displaced upon Ca^{2+}influx by Ca^{2+}/CaM.

Collectively, our previous and current data support the following model (Figure 9H): under basal conditions, apo-CaM and α-actinin bind to the same segment in $Ca_v1.2$, with the latter anchoring $Ca_v1.2$ via the cortical F-actin at the cell surface. Ca^{2+} influx has three effects: 1. Apo-CaM will bind Ca^{2+} and trigger a conformational change in $Ca_v1.2$ that will cause CDI within milliseconds. 2. At the same time Ca^{2+}/CaM will dislodge α-actinin from $Ca_v1.2$. In parallel eIF3e will bind to the loop between domains II and III of $Ca_v1.2$, which may or may not be influenced by CaM and α-actinin. If α-actinin displacement lasts long enough (e.g., prolonged Ca^{2+} influx), the endocytic machinery (exemplified by the adaptor protein AP2) will bind to $Ca_v1.2$, thereby initiating endocytosis. This step might also depend on eIF3e. After endocytosis, $Ca_v1.2$ can be reinserted into the plasma membrane (see (Liu et al., 1994)) or degraded.

Ca^{2+} overload is detrimental to neuronal function and has been implicated in various neurological diseases (Disterhoft et al., 1994; Lee et al., 1999). Chronic increase in L-type channel activity contributes to the etiology of senile symptoms and Alzheimer's disease (Deyo et al., 1989; Disterhoft et al., 1994; Thibault and Landfield, 1996). Our work uncovered an unexpected, complex mechanism for down regulation of $Ca_V1.2$ via Ca^{2+}-CaM-driven displacement of α-actinin and the ensuing internalization of $Ca_V1.2$. Dysregulation of this mechanism could contribute to those neurological diseases. These findings provide the basis for further mechanistic studies on surface localization of $Ca_V1.2$ under physiological and pathological conditions.

EXPERIMENTAL PROCEDURES

Animal Handling

All animal procedures were consistent with NIH guidelines and approved by the University of Iowa, UC Davis, University of North Carolina, and Stanford University Institutional Animal Care and Use Committees.

Immunoprecipitation and Immunoblotting from Brain Extract and Acute Forebrain Slices

Acute forebrain slices were prepared and handled as described (Halt et al., 2012). Rat brain tissue, forebrain slices, or HEK293 cells were extracted with 1% Triton X-100, cleared by 15–30 min ultracentrifugation (250,000 × *g*), and analyzed by IP and IB as described (Hall et al., 2007; Hall et al., 2006; Hell et al., 1993a).

Cell culture and imaging

Primary hippocampal neuronal cultures were prepared from E17–19 embryonic rats as described (Chen et al., 2008). HEK293 cells and neurons were seeded onto poly-L-lysine coated coverslips, transfected after 24 hrs and 6–12 DIV, respectively, using standard transfection reagents, and fixed after an additional 1–10 days for immunofluorescence analysis or used for recording of $I_{Ca,L}$ after 1 day.

Perfusion and immunofluorescence imaging of brain sections

Adult male rats were deeply anesthetized with sodium pentobarbital and perfused with 0.5% paraformaldehyde. Immunofluorescence was performed on Vibratome brain sections and images collected on a Leica SP2 confocal microscope.

In vitro pulldown assays

Expression and purification of MBP-tagged α-actinin-1 was according to the manufacturer's protocol for the pMalE-c2 vector (New England Biolabs). Expression, purification, and pull down of GST fusion proteins were as described previously (Hall et al., 2007; Hall et al., 2006).

Electrophysiology

For recording of I_{Ba} from HEK cells, extracellular solution contained (in mM) 125 NaCl, 10 tetraethylammonium chloride (TEA-Cl), 5 $BaCl_2$, 5.4 CsCl, 1,4-aminopyridine, 1 $MgCl_2$, 10 HEPES, 10 glucose (pH 7.4 with NaOH) and intracellular solution 120 CsCl, 10 TEA-Cl, 10 EGTA, 1 $MgCl_2$, 3 MgATP, 0.5 Na_3GTP, 10 HEPES (pH 7.3 with CsOH). For I_{Ca}, extracellular solution contained (in mM) 150 Tris, 1 $MgCl_2$, and 10 $CaCl_2$ and intracellular solution 140 *N*-methyl-D-glucamine, 10 HEPES, 1 $MgCl_2$, 2 Mg-ATP, 5 EGTA (pH 7.3 with methanesulfonic acid($MeSO_4$)). I_{Ba} or I_{Ca} were determined during a pulse protocol from a holding potential −70 mV to 0 or 10 mV.

For recording of $I_{Ca,L}$ from hippocampal neurons (14–21 DIV) extracellular solution contained (in mM) 130 N-methyl-D-glucamine (NMDG) Cl, 10 $CaCl_2$, 10 HEPES, 1 $MgCl_2$, and 10 glucose, (pH 7.4 with NMDG) plus 1 μM ω-conotoxin (CTx) MVIIC, 1 μM ω-CTxGVIA, and 30 μM niflumic acid and intracellular solution 110 Cs-$MeSO_4$, 20 TEA-Cl, 10 HEPES, 5 Mg-ATP, 0.5 GTP (pH 7.3 with CsOH).

Supplementary Material

Refer to Web version on PubMed Central for supplementary material.

Acknowledgments

This work was supported by the NIH training grants HL07121, DK07759, and AG00213 to DDH; AG017502 to JWH; NS35527 to RJW; DC009433 and HL087120 to AL; and the American Heart Association grant 0535235N (DDH). The authors thank Jason Ulrich, Audrey Dickey, Ivar Stein, and Coleen Cowan for technical support and M. Navedo, UC Davis, for critically reading the manuscript.

References

Allison DW, Gelfand VI, Spector I, Craig AM. Role of actin in anchoring postsynaptic receptors in cultured hippocampal neurons: differential attachment of NMDA versus AMPA receptors. J Neurosci. 1998; 18:2423–2436. [PubMed: 9502803]

Altier C, Garcia-Caballero A, Simms B, You H, Chen L, Walcher J, Tedford HW, Hermosilla T, Zamponi GW. The Ca_V beta subunit prevents RFP2-mediated ubiquitination and proteasomal degradation of L-type channels. Nat Neurosci. 2011; 14:173–180. [PubMed: 21186355]

Bartos JA, Ulrich JD, Li H, Beazely MA, Chen Y, Macdonald JF, Hell JW. Postsynaptic clustering and activation of Pyk2 by PSD-95. J Neurosci. 2010; 30:449–463. [PubMed: 20071509]

Berkefeld H, Sailer CA, Bildl W, Rohde V, Thumfart JO, Eble S, Klugbauer N, Reisinger E, Bischofberger J, Oliver D, et al. BKCa-Cav channel complexes mediate rapid and localized Ca2+-activated K^+ signaling. Science. 2006; 314:615–620. [PubMed: 17068255]

Bloodgood BL, Sabatini BL. Nonlinear regulation of unitary synaptic signals by Ca_V(2.3) voltage-sensitive calcium channels located in dendritic spines. Neuron. 2007; 53:249–260. [PubMed: 17224406]

Boudreau AC, Wolf ME. Behavioral sensitization to cocaine is associated with increased AMPA receptor surface expression in the nucleus accumbens. J Neurosci. 2005; 25:9144–9151. [PubMed: 16207873]

Chen Y, Stevens B, Chang J, Milbrandt J, Barres BA, Hell JW. NS21: redefined and modified supplement B27 for neuronal cultures. J Neurosci Methods. 2008; 171:239–247. [PubMed: 18471889]

Dai S, Hall DD, Hell JW. Supramolecular Assemblies and Localized Regulation of Voltage-gated Ion Channels. Physiol Rev. 2009; 89:411–452. [PubMed: 19342611]

Davare MA, Avdonin V, Hall DD, Peden EM, Burette A, Weinberg RJ, Horne MC, Hoshi T, Hell JW. A beta2 adrenergic receptor signaling complex assembled with the Ca^{2+} channel Ca_V1.2. Science. 2001; 293:98–101. [PubMed: 11441182]

Deyo RA, Straube KT, Disterhoft JF. Nimodipine facilitates associative learning in aging rabbits. Science. 1989; 243:809–811. [PubMed: 2916127]

Disterhoft, JF.; Gispen, WH.; Traber, J.; Khachaturian, ZS., editors. Calcium Hypothesis of Aging and Dementia. 1994.

Dolmetsch RE, Pajvani U, Fife K, Spotts JM, Greenberg ME. Signaling to the nucleus by an L-type calcium channel-calmodulin complex through the MAP kinase pathway. Science. 2001; 294:333–339. [PubMed: 11598293]

Dolphin AC. Calcium channel diversity: multiple roles of calcium channel subunits. Curr Op Neurobiol. 2009; 19:237–244. [PubMed: 19559597]

Dzhura I, Wu Y, Colbran RJ, Corbin JD, Balser JR, Anderson ME. Cytoskeletal disrupting agents prevent calmodulin kinase, IQ domain and voltage-dependent facilitation of L-type Ca^{2+} channels. J Physiol. 2002; 545:399–406. [PubMed: 12456820]

Fallon JL, Halling DB, Hamilton SL, Quiocho FA. Structure of calmodulin bound to the hydrophobic IQ domain of the cardiac Ca(v)1.2 calcium channel. Structure. 2005; 13:1881–1886. [PubMed: 16338416]

Gao T, Bunemann M, Gerhardstein BL, Ma H, Hosey MM. Role of the C terminus of the alpha 1C (Ca_V1.2) subunit in membrane targeting of cardiac L-type calcium channels. J Biol Chem. 2000; 275:25436–25444. [PubMed: 10816591]

Graef IA, Mermelstein PG, Stankunas K, Neilson JR, Deisseroth K, Tsien RW, Crabtree GR. L-type calcium channels and GSK-3 regulate the activity of NF-ATc4 in hippocampal neurons. Nature. 1999; 401:703–708. [PubMed: 10537109]

Green EM, Barrett CF, Bultynck G, Shamah SM, Dolmetsch RE. The tumor suppressor eIF3e mediates calcium-dependent internalization of the L-type calcium channel $Ca_V1.2$. Neuron. 2007; 55:615–632. [PubMed: 17698014]

Grosshans DR, Clayton DA, Coultrap SJ, Browning MD. LTP leads to rapid surface expression of NMDA but not AMPA receptors in adult rat CA1. Nature Neurosci. 2002; 5:27–33. [PubMed: 11740502]

Grover LM, Teyler TJ. Two components of long-term potentiation induced by different patterns of afferent activation. Nature. 1990; 347:477–479. [PubMed: 1977084]

Hall DD, Davare MA, Shi M, Allen ML, Weisenhaus M, McKnight GS, Hell JW. Critical role of cAMP-dependent protein kinase anchoring to the L-type calcium channel $Ca_V1.2$ via A-kinase anchor protein 150 in neurons. Biochem. 2007; 46:1635–1646. [PubMed: 17279627]

Hall DD, Feekes JA, Arachchige Don AS, Shi M, Hamid J, Chen L, Strack S, Zamponi GW, Horne MC, Hell JW. Binding of protein phosphatase 2A to the L-type calcium channel $Ca_V1.2$ next to Ser1928, its main PKA site, is critical for Ser1928 dephosphorylation. Biochem. 2006; 45:3448–3459. [PubMed: 16519540]

Halling DB, Aracena-Parks P, Hamilton SL. Regulation of voltage-gated Ca^{2+} channels by calmodulin. Sci STKE. 2006; 2006:er1. [PubMed: 16685765]

Halt AR, Dallapiazza R, Yu H, Stein IS, Qian H, Junti S, Wojcik S, Brose N, Sliva A, Hell JW. CaMKII binding to GluN2B is Critical During Memory Consolidation. The EMBO J. 2012; 31:1203–1216. [PubMed: 22234183]

Hell JW, Westenbroek RE, Breeze LJ, Wang KKW, Chavkin C, Catterall WA. N-methyl-D-aspartate receptor-induced proteolytic conversion of postsynaptic class C L-type calcium channels in hippocampal neurons. Proc Natl Acad Sci USA. 1996; 93:3362–3367. [PubMed: 8622942]

Hell JW, Westenbroek RE, Warner C, Ahlijanian MK, Prystay W, Gilbert MM, Snutch TP, Catterall WA. Identification and differential subcellular localization of the neuronal class C and class D L-type calcium channel α1 subunits. J Cell Biol. 1993a; 123:949–962. [PubMed: 8227151]

Hell JW, Yokoyama CT, Wong ST, Warner C, Snutch TP, Catterall WA. Differential phosphorylation of two size forms of the neuronal class C L-type calcium channel α1 subunit. J Biol Chem. 1993b; 268:19451–19457. [PubMed: 8396138]

Higley MJ, Sabatini BL. Calcium signaling in dendrites and spines: practical and functional considerations. Neuron. 2008; 59:902–913. [PubMed: 18817730]

Hoogland TM, Saggau P. Facilitation of L-type Ca2+ channels in dendritic spines by activation of beta2 adrenergic receptors. J Neurosci. 2004; 24:8416–8427. [PubMed: 15456814]

Johnson BD, Byerly L. A cytoskeletal mechanism for Ca^{2+} channel metabolic dependence and inactivation by intracellular Ca^{2+} Neuron. 1993; 10:797–804. [PubMed: 8098608]

Kepplinger KJ, Kahr H, Forstner G, Sonnleitner M, Schindler H, Schmidt T, Groschner K, Soldatov NM, Romanin C. A sequence in the carboxy-terminus of the alpha(1C) subunit important for targeting, conductance and open probability of L-type Ca(2+) channels. FEBS Lett. 2000; 477:161–169. [PubMed: 10908714]

Kim J, Ghosh S, Nunziato DA, Pitt GS. Identification of the components controlling inactivation of voltage-gated Ca^{2+} channels. Neuron. 2004; 41:745–754. [PubMed: 15003174]

Krupp JJ, Vissel B, Thomas CG, Heinemann SF, Westbrook GL. Interactions of calmodulin and alpha-actinin with the NR1 subunit modulate Ca^{2+}-dependent inactivation of NMDA receptors. J Neurosci. 1999; 19:1165–1178. [PubMed: 9952395]

Lader AS, Kwiatkowski DJ, Cantiello HF. Role of gelsolin in the actin filament regulation of cardiac L-type calcium channels. Am J Physiol. 1999; 277:C1277–1283. [PubMed: 10600780]

Lee J-M, Zipfel GJ, Choi DW. The changing landscape of ischaemic brain injury mechanisms. Nature. 1999; 399(Suppl):A7–A14. [PubMed: 10392575]

Leonard AS, Bayer KU, Merrill MA, Lim IA, Shea MA, Schulman H, Hell JW. Regulation of calcium/calmodulin-dependent protein kinase II docking to N-methyl-D-aspartate receptors by calcium/calmodulin and a-actinin. J Biol Chem. 2002; 277:48441–48448. [PubMed: 12379661]

Liu G, Shi J, Yang L, Cao L, Park SM, Cui J, Marx SO. Assembly of a Ca(2+)-dependent BK channel signaling complex by binding to beta2 adrenergic receptor. EMBO J. 2004; 23:2196–2205. [PubMed: 15141163]

Liu J, Bangalore R, Rutledge A, Triggle DJ. Modulation of L-type Ca^{2+} channels in clonal rat pituitary cells by membrane depolarization. Mol Pharmacol. 1994; 45:1198–1206. [PubMed: 8022413]

Lu L, Zhang Q, Timofeyev V, Zhang Z, Young JN, Shin HS, Knowlton AA, Chiamvimonvat N. Molecular coupling of a Ca^{2+}-activated K+ channel to L-type Ca^{2+} channels via alpha-actinin2. Circ Res. 2007; 100:112–120. [PubMed: 17110593]

Marrion NV, Tavalin ST. Selective activation of Ca^{2+}-activated K^{+} channels by co-localized Ca^{2+}channels in hippocampal neurons. Nature. 1998; 395:900–905. [PubMed: 9804423]

Merrill MA, Malik Z, Akyol Z, Bartos JA, Leonard AS, Hudmon A, Shea MA, Hell JW. Displacement of alpha-Actinin from the NMDA Receptor NR1 C0 Domain By Ca(2+)/Calmodulin Promotes CaMKII Binding. Biochem. 2007; 46:8485–8497. [PubMed: 17602661]

Moosmang S, Haider N, Klugbauer N, Adelsberger H, Langwieser N, Muller J, Stiess M, Marais E, Schulla V, Lacinova L, et al. Role of hippocampal Cav1.2 Ca^{2+} channels in NMDA receptor-independent synaptic plasticity and spatial memory. J Neurosci. 2005; 25:9883–9892. [PubMed: 16251435]

Nakamura M, Sunagawa M, Kosugi T, Sperelakis N. Actin filament disruption inhibits L-type Ca(2+) channel current in cultured vascular smooth muscle cells. Am J Physiol Cell Physiol. 2000; 279:C480–487. [PubMed: 10913014]

Obermair GJ, Szabo Z, Bourinet E, Flucher BE. Differential targeting of the L-type Ca2+ channel alpha1C ($Ca_V1.2$) to synaptic and extrasynaptic compartments in hippocampal neurons. Eur J Neurosci. 2004; 19:2109–2122. [PubMed: 15090038]

Pavalko FM, Burridge K. Disruption of the actin cytoskeleton after microinjection of proteolytic fragments of alpha-actinin. J Cell Biol. 1991; 114:481–491. [PubMed: 1907287]

Peng J, Kim MJ, Cheng D, Duong DM, Gygi SP, Sheng M. Semiquantitative proteomic analysis of rat forebrain postsynaptic density fractions by mass spectrometry. J Biol Chem. 2004; 279:21003–21011. [PubMed: 15020595]

Peterson BZ, DeMaria CD, Adelman JP, Yue DT. Calmodulin is the Ca^{2+} sensor for Ca^{2+}-dependent inactivation of L-type calcium channels. Neuron. 1999; 22:549–558. [PubMed: 10197534]

Pitt GS, Zuhlke RD, Hudmon A, Schulman H, Reuter H, Tsien RW. Molecular basis of calmodulin tethering and Ca2+-dependent inactivation of L-type Ca2+ channels. J Biol Chem. 2001; 276:30794–30802. [PubMed: 11408490]

Ravindran A, Lao QZ, Harry JB, Abrahimi P, Kobrinsky E, Soldatov NM. Calmodulin-dependent gating of Ca(v)1.2 calcium channels in the absence of Ca(v)beta subunits. Proc Natl Acad Sci USA. 2008; 105:8154–8159. [PubMed: 18535142]

Rosenmund C, Westbrook GL. Calcium-induced actin depolymerization reduces NMDA channel activity. Neuron. 1993; 10:805–814. [PubMed: 7684233]

Schnizler MK, Schnizler K, Zha XM, Hall DD, Wemmie JA, Hell JW, Welsh MJ. The cytoskeletal protein alpha-actinin regulates acid-sensing ion channel 1a through a C-terminal interaction. J Biol Chem. 2009; 284:2697–2705. [PubMed: 19028690]

Seisenberger C, Specht V, Welling A, Platzer J, Pfeifer A, Kuhbandner S, Striessnig J, Klugbauer N, Feil R, Hofmann F. Functional embryonic cardiomyocytes after disruption of the L-type alpha1C ($Ca_V1.2$) calcium channel gene in the mouse. J Biol Chem. 2000; 275:39193–39199. [PubMed: 10973973]

Sinnegger-Brauns MJ, Hetzenauer A, Huber IG, Renstrom E, Wietzorrek G, Berjukov S, Cavalli M, Walter D, Koschak A, Waldschutz R, et al. Isoform-specific regulation of mood behavior and pancreatic beta cell and cardiovascular function by L-type Ca^{2+} channels. J Clin Invest. 2004; 113:1430–1439. [PubMed: 15146240]

Tavalin SJ, Shepherd D, Cloues RK, Bowden SE, Marrion NV. Modulation of single channels underlying hippocampal L-type current enhancement by agonists depends on the permeant ion. J Neurophysiol. 2004; 92:824–837. [PubMed: 15056682]

Thibault O, Landfield PW. Increase in single L-type calcium channels in hippocampal neurons during aging. Science. 1996; 272:1017–1020. [PubMed: 8638124]

Tippens AL, Pare JF, Langwieser N, Moosmang S, Milner TA, Smith Y, Lee A. Ultrastructural evidence for pre- and postsynaptic localization of Cav1.2 L-type Ca^{2+} channels in the rat hippocampus. J Comp Neurol. 2008; 506:569–583. [PubMed: 18067152]

Van Petegem F, Chatelain FC, Minor DL Jr. Insights into voltage-gated calcium channel regulation from the structure of the $Ca_V1.2$ IQ domain-Ca^{2+}/calmodulin complex. Nat Struct Mol Biol. 2005; 12:1108–1115. [PubMed: 16299511]

Waithe D, Ferron L, Page KM, Chaggar K, Dolphin AC. β-Subunits Promote the Expression of $Ca_V2.2$ Channels by Reducing Their Proteasomal Degradation. J Biol Chem. 2011; 286:9598–9611. [PubMed: 21233207]

Walikonis RS, Jensen ON, Mann M, Provance DW Jr, Mercer JA, Kennedy MB. Identification of proteins in the postsynaptic density fraction by mass spectrometry. J Neurosci. 2000; 20:4069–4080. [PubMed: 10818142]

Walikonis RS, Oguni A, Khorosheva EM, Jeng CJ, Asuncion FJ, Kennedy MB. Densin-180 forms a ternary complex with the (alpha)-subunit of Ca^{2+}/calmodulin-dependent protein kinase II and (alpha)-actinin. J Neurosci. 2001; 21:423–433. [PubMed: 11160423]

Wang HG, George MS, Kim J, Wang C, Pitt GS. Ca^{2+}/calmodulin regulates trafficking of Ca(V)1.2 Ca^{2+} channels in cultured hippocampal neurons. J Neurosci. 2007; 27:9086–9093. [PubMed: 17715345]

Wyszynski M, Kharazia V, Shanghvi R, Rao A, Beggs AH, Craig AM, Weinberg R, Sheng M. Differential regional expression and ultrastructural localization of alpha-actinin-2, a putative NMDA receptor-anchoring protein, in rat brain. J Neurosci. 1998; 18:1383–1392. [PubMed: 9454847]

Wyszynski M, Lin J, Rao A, Nigh E, Beggs AH, Craig AM, Sheng M. Competitive binding of α-actinin and calmodulin to the NMDA receptor. Nature. 1997; 385:439–442. [PubMed: 9009191]

Xu X, Marx SO, Colecraft HM. Molecular mechanisms, and selective pharmacological rescue, of Rem-inhibited $Ca_V1.2$ channels in heart. Circ Res. 2010; 107:620–630. [PubMed: 20616312]

Zhang J, Bal M, Bierbower S, Zaika O, Shapiro MS. AKAP79/150 Signal Complexes in G-Protein Modulation of Neuronal Ion Channels. J Neurosci. 2011; 31:7199–7211. [PubMed: 21562284]

Zhang S, Ehlers MD, Bernhardt JP, Su CT, Huganir RL. Calmodulin mediates calcium-dependent inactivation of N-methyl-D-aspartate receptors. Neuron. 1998; 21:443–453. [PubMed: 9728925]

Zhang W, Gunst SJ. Dynamic association between alpha-actinin and beta-integrin regulates contraction of canine tracheal smooth muscle. J Physiol. 2006; 572:659–676. [PubMed: 16513669]

Zhou J, Olcese R, Qin N, Noceti F, Birnbaumer L, Stefani E. Feedback inhibition of Ca^{2+} channels by Ca^{2+} depends on a short sequence of the C terminus that does not include the Ca^{2+} -binding function of a motif with similarity to Ca^{2+} -binding domains. Proc Natl Acad Sci USA. 1997; 94:2301–2305. [PubMed: 9122189]

Zuhlke RD, Pitt GS, Deisseroth K, Tsien RW, Reuter H. Calmodulin supports both inactivation and facilitation of L-type calcium channels. Nature. 1999; 399:159–162. [PubMed: 10335846]

HIGHLIGHTS

- α-Actinin binding to $Ca_V1.2$ IQ region maintains $Ca_V1.2$ surface and spine localization
- Ca^{2+} influx via L channels, not NMDAR, displaces α-actinin from $Ca_V1.2$ via calmodulin
- Ca^{2+} influx via L channels results in loss of $Ca_V1.2$ from dendritic spines
- This Ca^{2+} influx causes run down of L current by calmodulin-induced endocytosis.

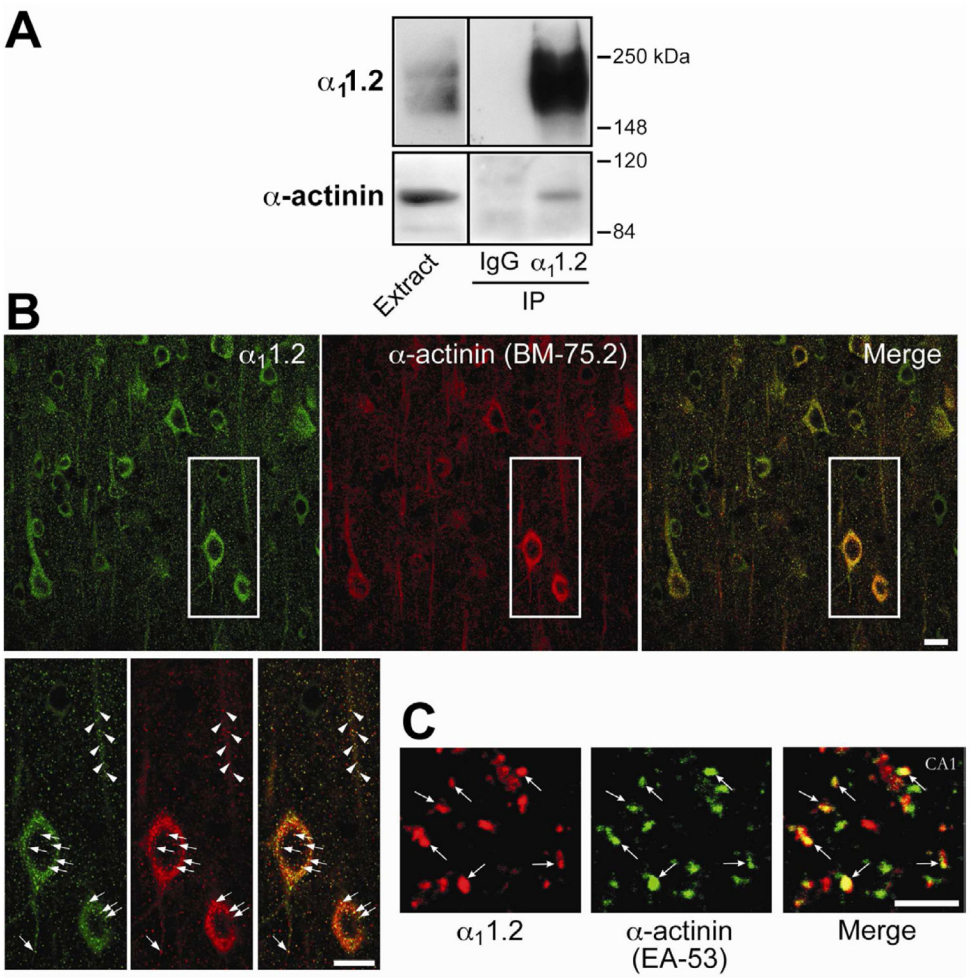

Figure 1. α-Actinin Interacts and Colocalizes with $Ca_V1.2$ in Neurons

(A) CoIP of α-actinin with $Ca_v1.2$ from Triton X-100 solubilized rat forebrain.

(B) Confocal images from murine cortical slices showing colocalization between $\alpha_1$1.2 and α-actinin within the soma (arrows) and neurites (arrowheads) of cortical neurons. Bottom left panels show a magnified view of the area indicated in the top row panels.

(C) Confocal images from the CA1 region of the hippocampus in rat brain slices.

Scale bars: B: 20 μm; C: 10 μm. See Figure S1 for antibody specificity.

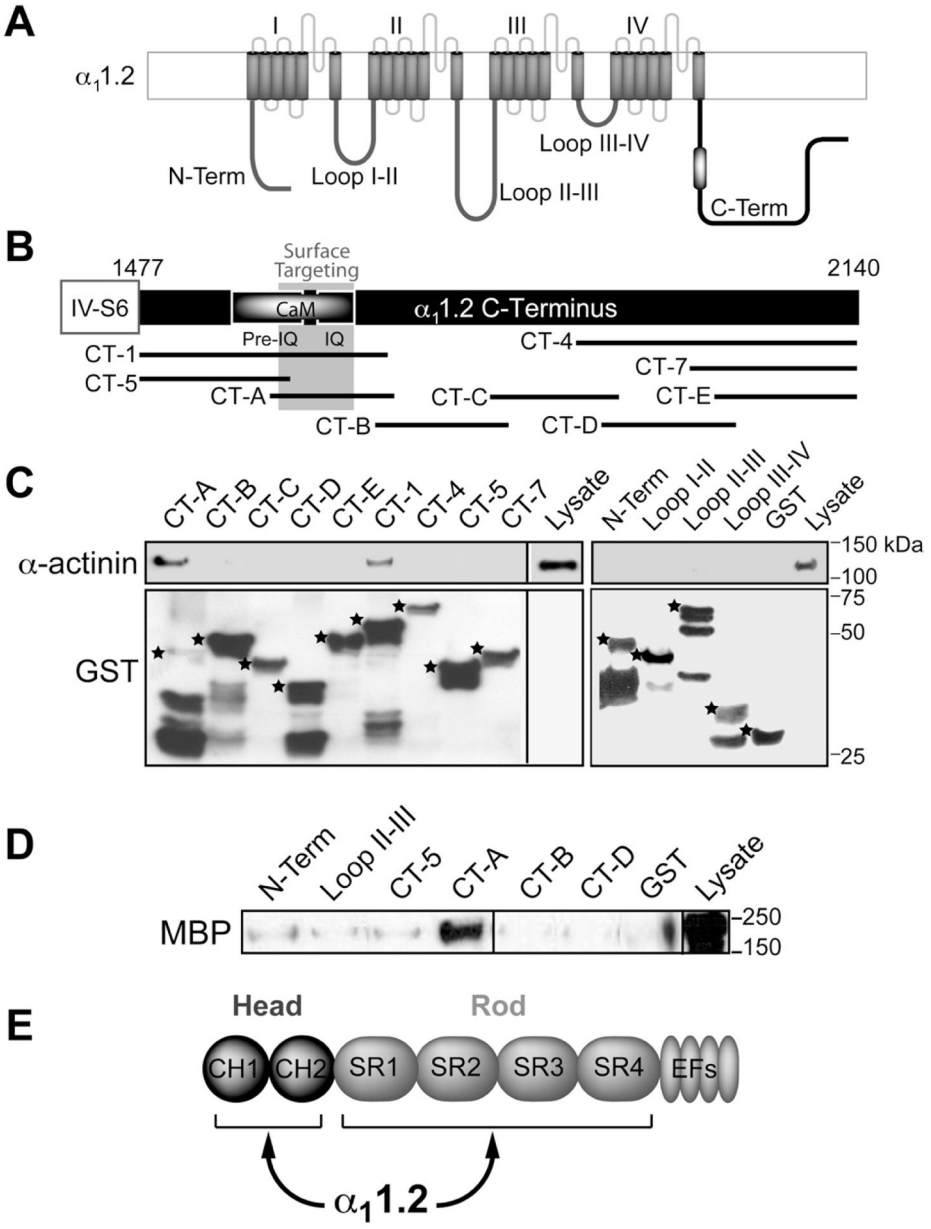

Figure 2. α-Actinin-1 Interacts with the CaM Binding and Surface Targeting Region of the $\alpha_1$1.2 C-terminus

(A) Diagram of $\alpha_1$1.2 depicts intracellular N- and C-termini and four homologous domains, which form the channel pore and are connected by intracellular loops. Black and white oval: Pre-IQ + IQ region.

(B) Diagram of the $\alpha_1$1.2 C-terminus depicts the Pre-IQ + IQ CaM binding region, the surface targeting region (residues 1626–1666 (Gao et al., 2000)), and the overlapping C-terminal GST fusion proteins used.

(C) IB of α-actinin pull-down from rat forebrain homogenates by indicated GST fusion proteins. Top, probing for α-actinin binding to GST fusion proteins. α-actinin bound to CT-1 [corresponding to rabbit $\alpha_1$1.2 residues 1507–1733 (NFDYL…GGLFG)] and to CT-A

[corresponding to rat $\alpha_1$1.2 residues 1584–1707 (ELRAI…FGNHV); the latter are homologous to rabbit residues 1614–1737; the change in numbering is because the rat sequence lacks 30 residues at the very N-terminus compared to rabbit]. Bottom, probing for total GST fusion protein present within each pull-down reaction. While there are comparable amounts of expected full length forms for most fusion proteins (*), the C-terminal half of CT-A is largely removed identifying the N-terminal half as α-actinin binding site. In addition, the 20 residues at the N-terminus, which would overlap with the C-terminal 20 residues of CT-A, (SAASEDDIFRRAGGLFGNHV) do not apparently bind α-actinin.
(D) IB of pull-down of purified MBP-α-actinin-1 by immobilized $\alpha_1$1.2 GST fusion proteins using an anti-MBP antibody. CT-A directly interacts with α-actinin.
(E) Schematic illustrates head and rod domain of α-actinin.
See also Table S1 for details on subcloning.

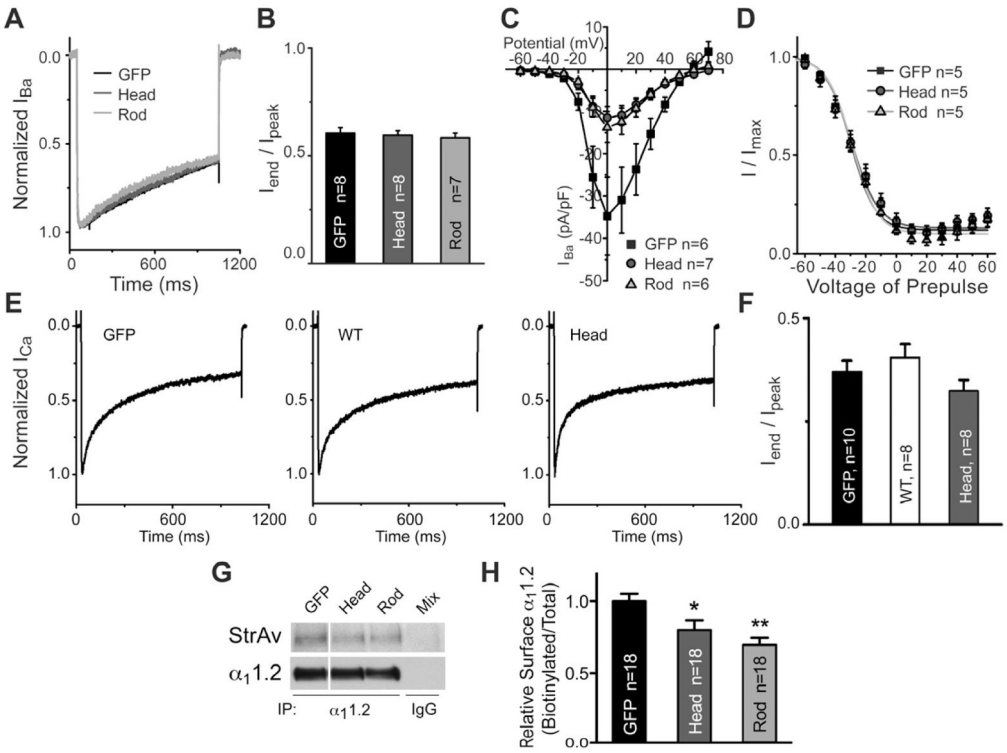

Figure 3. Dominant Negative α-Actinins Reduce Surface Expression of $Ca_V1.2$

HEK293 cells were transfected with $\alpha_1$1.2, $\alpha_2\delta_1$, β_{2a}, and either GFP, EGFP-α-actinin-1 or dominant negative EGFP-α-actinin-Head or -Rod constructs.

(A, E) Ba^{2+} (**A**) and Ca^{2+} (**E**) currents from GFP-positive cells were elicited from a holding potential of −80 mV by depolarization to +10 mV for 1 s. Current traces were normalized to their peak values and overlaid for comparison in **A**.

(B, F) Summary of the ratios of the Ba^{2+} (**B**) and Ca^{2+} (**F**) currents at the end of the 1 s depolarizing pulse to their peak values.

(C) I/V curves of Ba^{2+} peak currents activated from a holding potential of −70 mV by depolarization to the marked potentials for 300 ms (interpulse intervals were 10 s; $p<0.05$ for head and for rod vs. GFP control between −10 and +40 mV; t-test).

(D) Steady-state inactivation curves. Depolarizing pulses to the indicated potentials for 3 s were followed by a test pulse for 100 ms to the potential that elicited maximal peak currents (see I/V curves in **C**). Current values were normalized to the maximal current observed in each set of measurements, averaged, and fitted to the Boltzmann equation.

(B, C, D, F) Means ± SEM from n independent but interleaved transfection experiments.

(G) Surface biotinylation of $\alpha_1$1.2 in HEK293 cells. $Ca_V1.2$ was extracted with Triton X-100 before IP with anti-$\alpha_1$1.2, IB with anti-$\alpha_1$1.2, stripping, and reprobing with streptavidin. Mix, combination of lysates from the three samples after mock IP with nonspecific control IgG. Lanes for each probing were from the same immunoblot and exposure and rearranged for clarity.

(H) Means ± SD of relative ratios of biotinylated to total $\alpha_1$1.2 signals, normalized to control (GFP; n, number of independent samples from 10 different experiments; * $p<0.05$, ANOVA).

See also Figure S2 for lack of effect of head and rod domains on F actin.

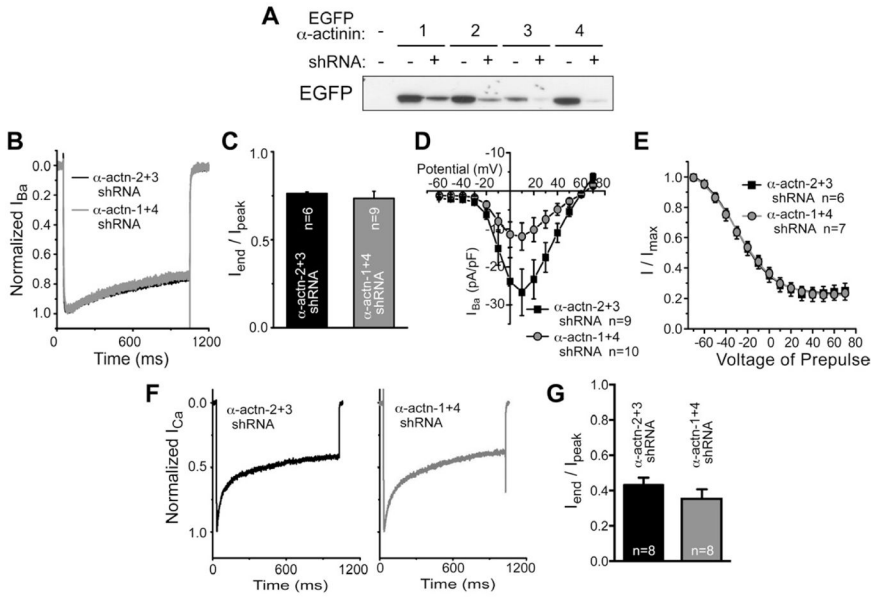

Figure 4. Knockdown of Endogenous α-Actinins Reduces $Ca_V1.2$ Current Density

(A) Knockdown of α-actinin isoforms with isoform-specific shRNA encoding vectors. HEK293 cells were cotransfected with EGFP-tagged α-actinins-1, -2, -3, or -4 and pSilencer-DsRed encoding no shRNA (−) or shRNA against the respective α-actinin isoforms (+). Lysate samples containing equal amounts of protein were analyzed by immunoblotting with anti-GFP antibodies for detection of the corresponding EGFP-tagged α-actinins.

(B–G) HEK293 cells were transfected with $\alpha_1$1.2, $\alpha_2\delta_1$, β_{2a} and a combination of pSilencer-DsRed with shRNA against α-actinins-1 and -4 to knock down endogenous α-actinin (Figure S3). A combination of shRNA against α-actinins-2 and -3 served as negative control.

(B, F) Ba^{2+} (**B**) and Ca^{2+} (**F**) currents from DsRed-positive cells were elicited from a holding potential of −80 mV by depolarization to +10 mV for 1 s. Current traces were normalized to their peak values and overlaid for comparison in **B**.

(C, G) Summary of the ratios of the Ba^{2+} (**C**) and Ca^{2+} (**G**) currents at the end of the 1 s depolarizing pulse to their peak values.

(D) I/V curves of Ba^{2+} peak currents activated from a holding potential of −70 mV by depolarization to the marked potentials for 300 ms (interpulse intervals were 10 s; $p<0.05$ for α-actinin-1+4 shRNA vs. α-actinin-2+3 shRNA control between +10 and +40 mV; t-test).

(E) Steady-state inactivation curves. Depolarizing pulses to the indicated potentials for 3 s were followed by a test pulse for 100 ms to the potential that elicited maximal peak currents (see I/V curves in **D**). Current values were normalized to the maximal current observed in each set of measurements, averaged, and fitted to the Boltzmann equation.

(C, D, E, G) Values are given as means ± SEM and are derived from n independent but interleaved transfection experiments.

See also Figure S3 for α-actinin isoforms in HEK293 cells and for lack of effect of shRNA on F-actin.

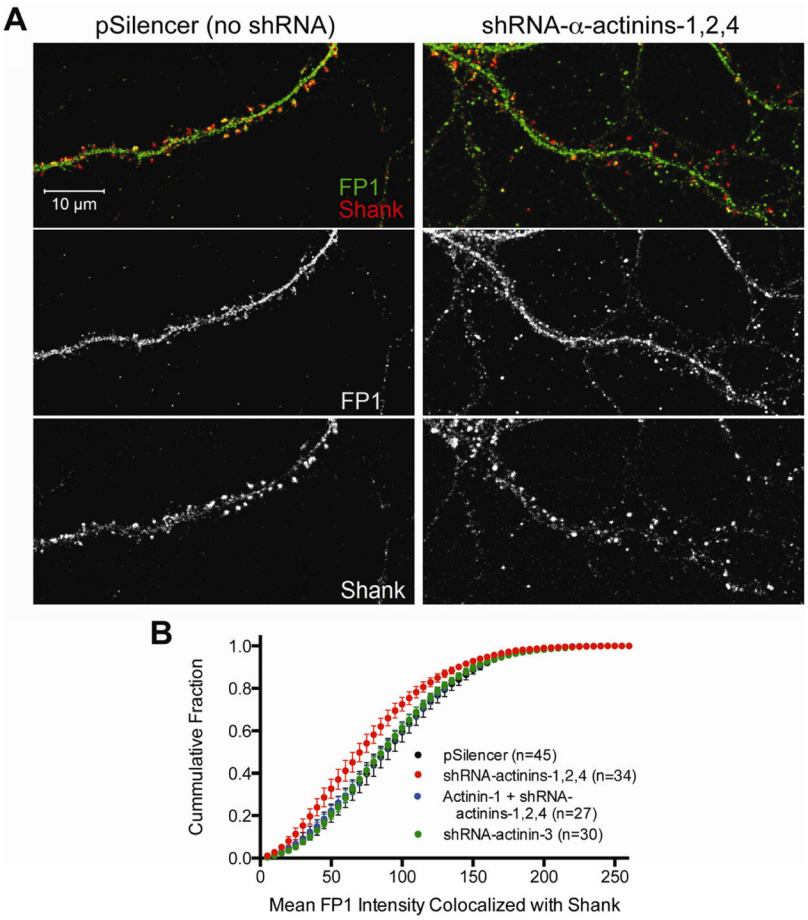

Figure 5. α-Actinin Knockdown Reduces $Ca_V1.2$ in Spines

Hippocampal cultures were transfected with parental pSilencer-DsRed, α-actinin-3 shRNA, or shRNAs against α-actinins-1, -2, and -4 alone or in combination with the α-actinin-1 rescue vector at 4 DIV and stained with FP1 and anti-Shank at 21 DIV.

(A) Confocal immunofluorescence micrographs.

(B) Cumulative fraction plot for $\alpha_1$1.2 intensity of puncta colocalized with the postsynaptic marker Shank. A total of n images were analyzed from 5 independent experiments ($p < 0.01$ for sh1/2/4 vs. control, vs. sh3, and vs. rescue by ANOVA; error bars indicate SEM).

See also Figure S4 for colocalization of $\alpha_1$1.2 and α-actinin.

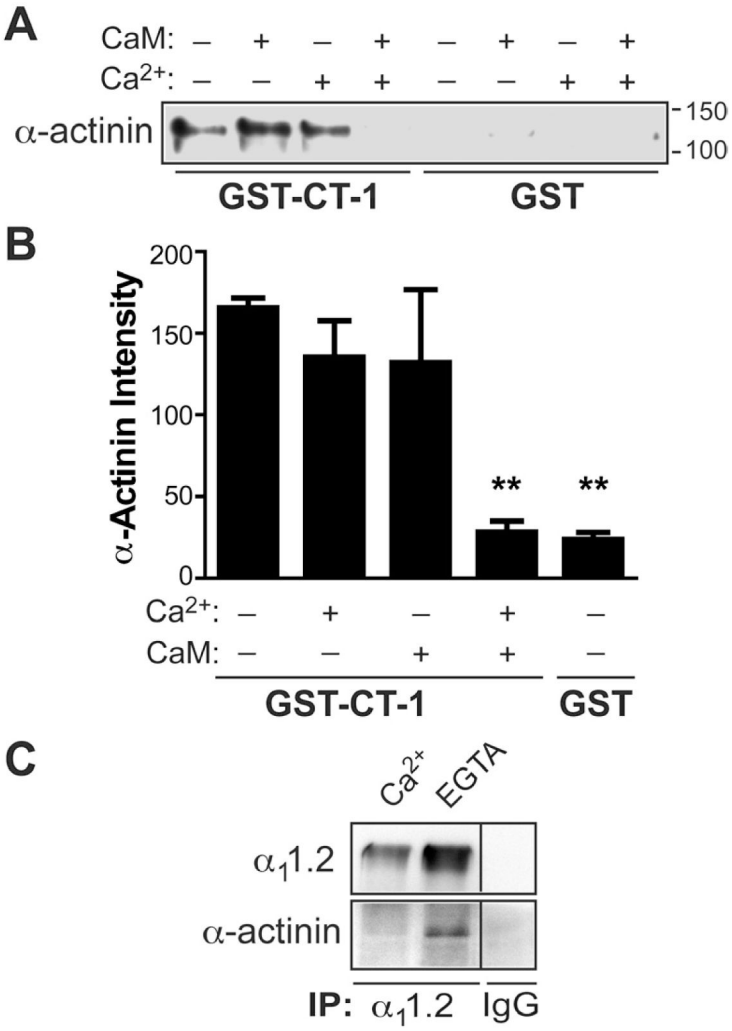

Figure 6. Both Ca^{2+} and CaM are Required to Displace α-Actinin from $α_1$1.2

(A,B) Purified GST or GST-CT-1 were immobilized on glutathione-Sepharose and incubated with MBP-α-actinin-1 and subsequently ± CaM in the presence of either 5 mM Ca^{2+} (Ca^{2+} +) or 500 μM EGTA (Ca^{2+} -) before IB for MBP **(A)** and densitometric quantification **(B)**. Only combined Ca^{2+}-CaM, but not Ca^{2+} or CaM alone, displaced α-actinin. (** $p<0.01$, ANOVA; n=6).

(C) CoIP of α-actinin and $α_1$1.2 is Ca^{2+} sensitive. Rat brain was extracted with Triton X-100 in the presence of 2.5 mM Ca^{2+} or 5 mM EGTA before IP. Pooled homogenates were used for control IP with non-specific IgG. IBs were probed for $α_1$1.2 (top) and α-actinin (bottom). α-actinin co-precipitated with $α_1$1.2 only in the absence of free Ca^{2+}.

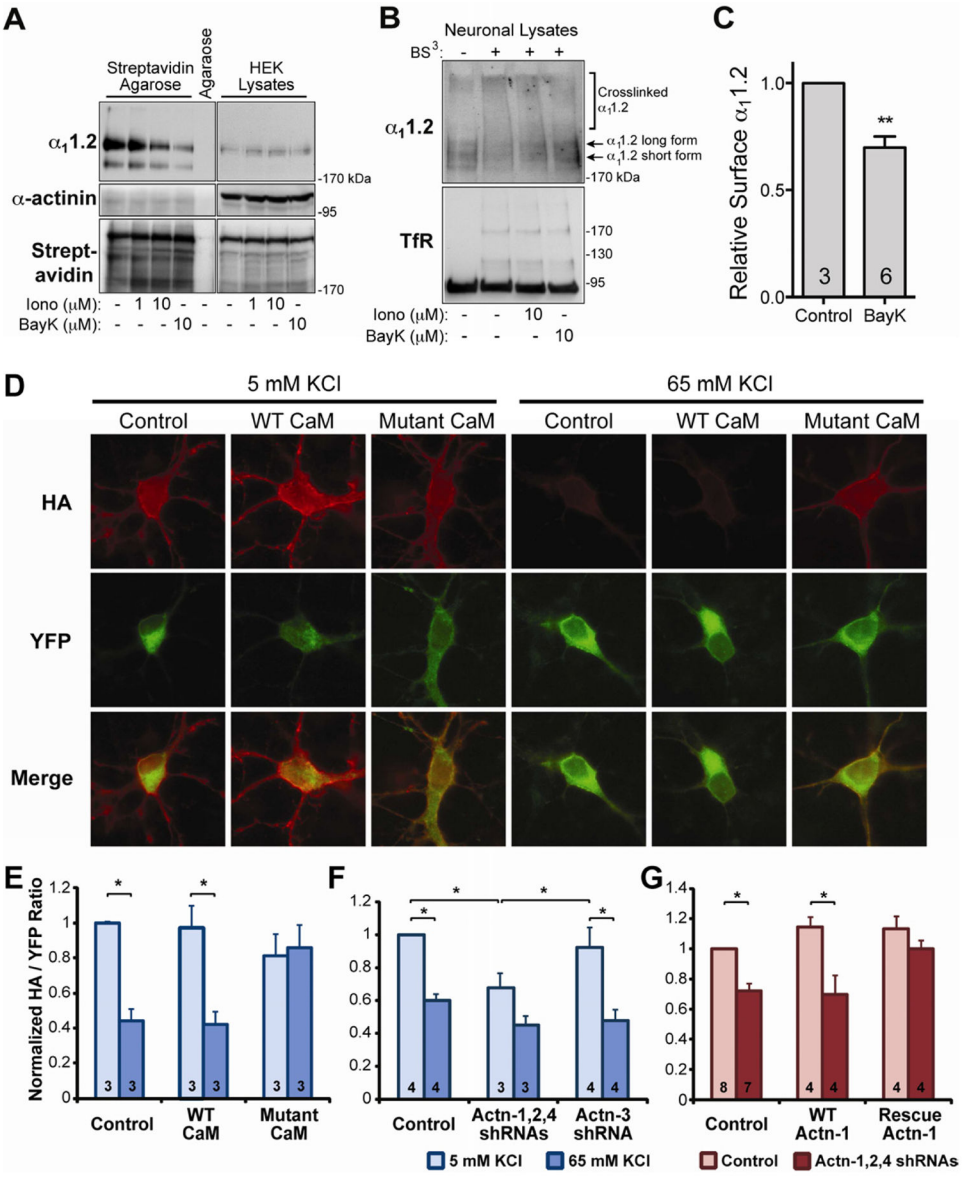

Figure 7. Ca^{2+} Influx Decreases $Ca_V1.2$ on the Surface of HEK293 Cells and Neurons

(A) HEK293 cells were transfected with $\alpha_1$1.2, β_{2a}, and $\alpha_2\delta_1$ and treated with ionomycin or BayK8644 for 10 min. Surface proteins were biotinylated, extracted with Triton X-100, and pulled down with streptavidin Agarose before IB for $\alpha_1$1.2 (top), α-actinin (middle), and total biotinylated proteins (bottom).

(B) IB of surface vs. internal $\alpha_1$1.2 (top) and transferrin receptor (TfR, bottom) from 21 DIV primary cortical neurons treated with ionomycin and BayK8644. Surface proteins crosslinked by BS^3 are shifted towards the top of blots.

(C) Quantification of $\alpha_1$1.2 from BayK8644 treated and BS^3 crosslinked neurons from 3 independent experiments. BayK8644 significantly induced $Ca_V1.2$ internalization as measured by the decrease in crosslinked to uncrosslinked $\alpha_1$1.2 signal ($p<0.01$, t-test; n, number of independent samples from 3 experiments).

(D–G) Hippocampal neurons were cotransfected with $Ca_V1.2$ (YFP-HA-$\alpha_1$1.2) and CaM, shRNA, or α-actinin constructs as indicated. After 48 h, neurons were depolarized with control (5 mM) or high (65 mM) KCl for 15 min, fixed, and stained for surface-expressed $Ca_V1.2$ with anti-HA antibody.

(D) Surface-labeled (HA, red) vs total expression (YFP, green) of HA-$\alpha_1$1.2-YFP after coexpression with none, WT or mutant CaM_{1234} ± depolarization with 65 mM KCl.

(**E–G)** Quantification of $Ca_V1.2$ surface expression as the HA:YFP signal ratio normalized to basal expression with control vector cotransfection. Thirty neurons were analyzed from each of 3–8 independent experiments (indicated within bars; * $p < 0.05$, ANOVA; bars: SEM).

(E) Mutant CaM_{1234} but not WT CaM prevents depolarization-triggered internalization of $Ca_V1.2$.

(F) Knockdown of α-actinin with combined shRNA plasmids against α-actinin-1/2/4 but not shRNA against α-actinin-3, which neurons lack, reduces basal $Ca_V1.2$ surface expression and KCl-induced $Ca_V1.2$ endocytosis.

(G) Rescue of shRNA-induced decrease in basal $Ca_V1.2$ surface expression by ectopic expression of shRNA-insensitive α-actinin-1.

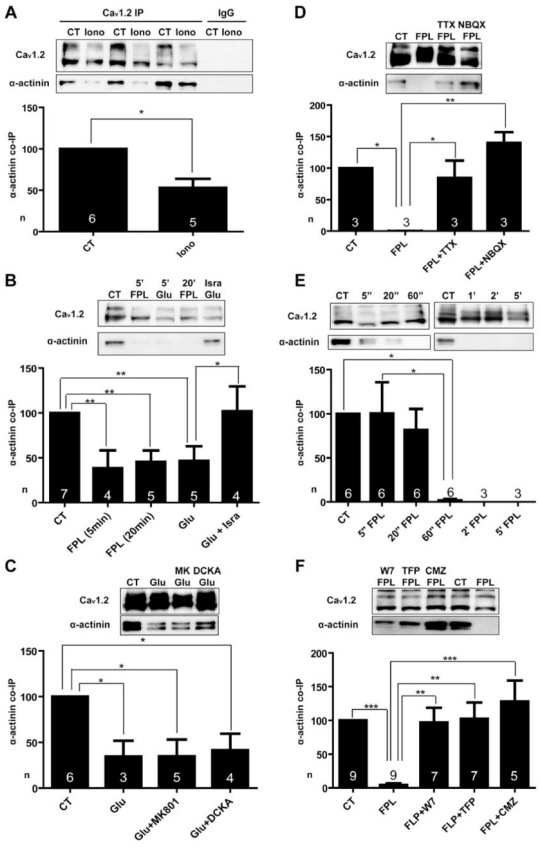

Figure 8. CaM Displaces α-Actinin from $Ca_V1.2$ upon Ca^{2+} Influx

Forebrain slices were pre-incubated for 5 min with vehicle or 20 μM isradipine, 10 μM MK801, 10 μM DCKA, 1 μM TTX, 10 μM NBQX, 10 μM W7, 20 μM TFP, or 30 μM calmidazolium (CMZ) if indicated, treated with vehicle (control, CT), 10 μM ionomycin, 20 μM FPL64176, or 100 μM glutamate for indicate time periods, and extracted with 1% Triton X-100 before IP of $Ca_V1.2$ and IB for $\alpha_1$1.2 and α-actinin.

(A) Ionomycin reduced coIP of α-actinin with $Ca_V1.2$.

(B) FPL and glutamate reduced coIP; the glutamate effect was prevented by the L-type channel blocker isradipine.

(C) The effect of 5 min glutamate treatment was not prevented by the two NMDAR inhibitors MK801 and DCKA.

(D) The effect of 5 min FPL treatment was prevented by reducing network activity with TTX or NBQX.

(E) The FPL effect was complete after 1 min.

(F) The effect of 5 min FPL treatment was prevented by three different CaM inhibitors.

(A–F) Bars are mean±SEM from n samples in ≥ 3 experiments (*p<0.05, **p<0.01, ***p<0.001).

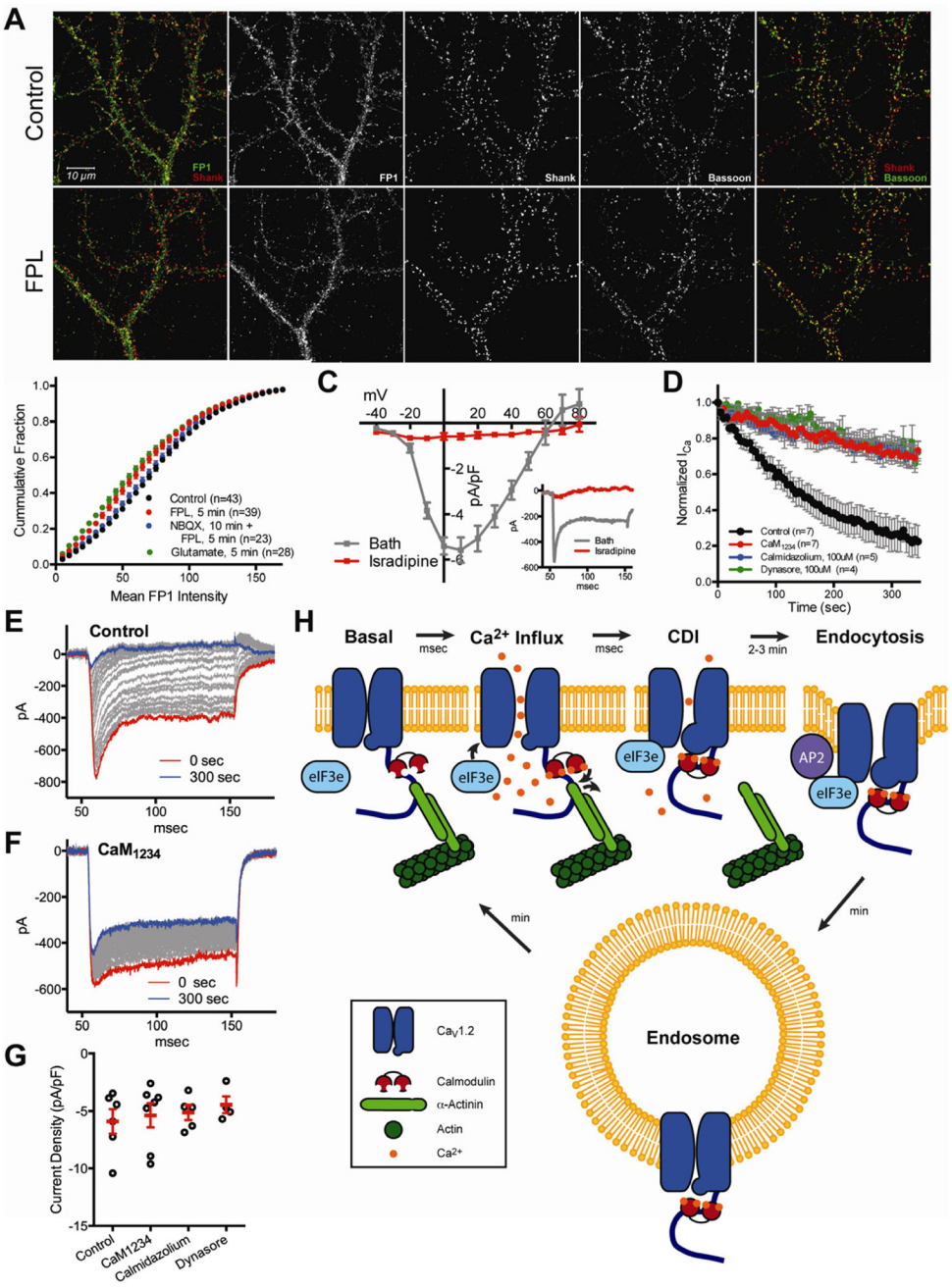

Figure 9. CaM is Necessary for $Ca_V1.2$ Endocytosis upon Ca^{2+} Influx

(A, B) Hippocampal cultures (21 DIV) were treated with vehicle, FPL ± NBQX, or glutamate for 5 min and stained with FP1, anti-Shank, and anti-bassoon.

(A) Confocal immunofluorescence micrographs.

(B) Cumulative fraction plots for $\alpha_1$1.2 intensity of puncta colocalized with the postsynaptic marker Shank (left panels in **A**). Shank in turn colocalized with the presynaptic marker bassoon (right panels in **A**). A total of n images were analyzed from 5 independent experiments (Control vs. FPL and vs. glutamate: $p<0.001$; FPL+NBQX vs. FPL: $p < 0.05$; bars: SEM).

(C–G) L-type Ca^{2+} currents ($I_{Ca,L}$) were recorded from hippocampal neurons 14–21 DIV during depolarizing steps from a holding potential of −60 mV to the indicated potentials. 1 μM ω-conotoxin (CTx) MVIIC and 1 μM ω-CTxGVIA were present to block P/Q-type and N-type Ca^{2+} channels, respectively.

(C) I/V curves before and after perfusion with 10 μM of the L-type blocker isradipine. Inset shows recordings obtained during 100 ms-long depolarizations from −60 mV to 0 mV before and after application of 10 μM isradipine. The I/V curves are typical for L-type currents and the block of these currents by isradipine (inset) pharmacologically identifies those as L-type.

(D) Run down of $I_{Ca,L}$ in hippocampal neurons 14–21 DIV with 10 mM extracellular Ca^{2+} upon repeated 100 ms - depolarizations from −60 to 0 mV (Control) was largely prevented by expression of the Ca^{2+} binding deficient CaM_{1234} and inclusion of the CaM blocker calmidazolium and the endocytosis blocker dynasore. For each time course, peak $I_{Ca,L}$ values were normalized to the first trace.

(E, F) Complete set of current recordings over full time course of run down (red, initial trace; blue, last trace) for Control **(E)** and CaM_{1234} **(F)** which, as expected, also inhibited CDI but not VDI.

(G) Complete set of initial peak current densities, which were not different between control and various treatment conditions.

(H) Model of Ca^{2+}/CaM-mediated displacement of α-actinin and Ca^{2+}-induced endocytosis of $Ca_V1.2$. Under resting conditions α-actinin binds simultaneously with apo-CaM to the IQ motif of $\alpha_1 1.2$, tethering $Ca_v1.2$ to the cortical F-actin at the plasma membrane. Upon Ca^{2+} influx apo-CaM will bind Ca^{2+}, inducing a conformational change in $Ca_v1.2$ that will result in CDI within ms. Concurrently, Ca^{2+}/CaM will dislodge α-actinin from $Ca_v1.2$. At the same time eIF3e will bind to the loop between domains II and III of $\alpha_1 1.2$, which could, but does not have to, be regulated by CaM and α-actinin. If α-actinin remains detached from $Ca_v1.2$, the endocytic adaptor protein AP2 or other functionally related proteins bind to $Ca_v1.2$ to initiate endocytosis. This binding step might depend on eIF3e. After endocytosis, $Ca_v1.2$ can be reinserted into the plasma membrane or degraded.

See also Figure S5 for additional quantitative analysis of spine localization of $\alpha_1 1.2$.